Editors' Suggestion

Metallic and Deconfined Quantum Criticality in Dirac Systems

Zi Hong Liu,[1] Matthias Vojta,[2] Fakher F. Assaad,[1] and Lukas Janssen[2]
[1] *Institut für Theoretische Physik und Astrophysik and Würzburg-Dresden Cluster of Excellence ct.qmat, Universität Würzburg, 97074 Würzburg, Germany*
[2] *Institut für Theoretische Physik and Würzburg-Dresden Cluster of Excellence ct.qmat, Technische Universität Dresden, 01062 Dresden, Germany*

(Received 3 September 2021; accepted 25 January 2022; published 23 February 2022)

Motivated by the physics of spin-orbital liquids, we study a model of interacting Dirac fermions on a bilayer honeycomb lattice at half filling, featuring an explicit global $\mathrm{SO}(3) \times \mathrm{U}(1)$ symmetry. Using large-scale auxiliary-field quantum Monte Carlo (QMC) simulations, we locate two zero-temperature phase transitions as function of increasing interaction strength. First, we observe a continuous transition from the weakly interacting semimetal to a different semimetallic phase in which the SO(3) symmetry is spontaneously broken and where two out of three Dirac cones acquire a mass gap. The associated quantum critical point can be understood in terms of a Gross-Neveu-SO(3) theory. Second, we subsequently observe a transition toward an insulating phase in which the SO(3) symmetry is restored and the U(1) symmetry is spontaneously broken. While strongly first order at the mean-field level, the QMC data are consistent with a direct and continuous transition. It is thus a candidate for a new type of deconfined quantum critical point that features gapless fermionic degrees of freedom.

DOI: 10.1103/PhysRevLett.128.087201

Metallic quantum criticality corresponds to the spontaneous breaking of a symmetry in a metallic environment triggered by varying a nonthermal control parameter such as doping, magnetic field, or pressure [1–3]. Order-parameter fluctuations often induce non-Fermi-liquid behavior in a temperature-versus-control-parameter window of the phase diagram [4–6]. Metallic quantum criticality is pivotal in understanding anomalous transport and strange-metal behavior in strongly correlated materials, such as heavy-fermion compounds [7] and Cu- and Fe-based high-temperature superconductors [8,9]. In spite of extensive efforts [1–3,10–17], a controlled analytical treatment of this problem in the presence of a Fermi surface remains a major challenge. The main difficulty is to tame the strong quantum fluctuations that arise from the abundance of gapless particle-hole modes near the Fermi surface. From the numerical point of view [18], the fact that these transitions are characterized by dynamical critical exponents $z > 1$ impedes the ability to reach sufficiently low temperatures on large lattices [19].

Dirac systems, in contrast, have emergent Lorentz symmetry: Space and time are interchangeable and $z = 1$. Furthermore, instead of an extended Fermi surface, they feature isolated Fermi points. In the past years, there has been a considerable amount of work investigating dynamical mass generation in these systems. The understanding of such transitions relies on the Gross-Neveu-Yukawa theory, in which an order-parameter field of given symmetry is coupled to a fermion-mass term in the same symmetry sector [20]. Various instances of these transitions have been studied from the perspective of high-energy [21–25] and solid-state [26–36] physics. In all of the above examples, the quantum critical points separate Dirac semimetallic states from insulating states with a full gap in the fermionic spectrum. Dirac systems can, however, in principle, also support relativistic quantum critical points between two distinct semimetallic phases. This possibility was recently scrutinized in the context of a frustrated spin-orbital model, in which case the fermion degrees of freedom arise from a spin fractionalization mechanism [37]. If such a transition is realizable, it would represent a Dirac "avatar" of metallic quantum criticality that may be more easily accessible to both numerical and field-theoretical analyses.

In this Letter, we investigate a two-dimensional lattice model of interacting fermions designed to feature such a semimetal-to-semimetal quantum critical point. Inspired by Ref. [37], we study the Hamiltonian

$$H = -t \sum_{\langle \boldsymbol{i},\boldsymbol{j} \rangle} c^{\dagger}_{\boldsymbol{i}\sigma\lambda} c_{\boldsymbol{j}\sigma\lambda} - J \sum_{\boldsymbol{i}\alpha} \left(c^{\dagger}_{\boldsymbol{i}\sigma\lambda} K^{\alpha}_{\sigma\sigma'} \tau^{z}_{\lambda\lambda'} c_{\boldsymbol{i}\sigma'\lambda'} \right)^2, \qquad (1)$$

where $\langle \boldsymbol{i},\boldsymbol{j} \rangle$ denote pairs of nearest-neighbor sites of a honeycomb lattice, $\lambda = 1, 2$ is an additional layer index, and summation over repeated indices is implied. Further, $\sigma = 1, 2$, and 3 is a SO(3) flavor index, $(K^{\alpha})_{\sigma\sigma'} = -i\epsilon_{\alpha\sigma\sigma'}$ are the generators of SO(3), and $\tau^{x,y,z}$ are Pauli matrices. The model is particle-hole symmetric such that zero chemical potential corresponds to half filling.

0031-9007/22/128(8)/087201(6)

The interaction term in Eq. (1) is chosen such that the SO(3) symmetry may be spontaneously broken, resulting in a three-component order parameter $\boldsymbol{m} = (m_1, m_2, m_3)^\top$. For a single layer, this leads to the low-energy effective Hamiltonian

$$\mathcal{H} = \Psi_\sigma^\dagger[i\gamma_0\gamma_j p_j \delta_{\sigma\sigma'} + m_\alpha (K^\alpha)_{\sigma\sigma'}\gamma_0]\Psi_{\sigma'}, \qquad (2)$$

where $i\gamma_0\gamma_j p_j$ is the usual Dirac Hamiltonian in two spatial dimensions, $j = 1, 2$. The operator $\boldsymbol{K}_{\sigma\sigma'}\gamma_0$ anticommutes with the Dirac Hamiltonian and, as such, may be thought of as a mass term, but since $(\boldsymbol{m}\cdot\boldsymbol{K})\boldsymbol{v} = i\boldsymbol{m}\times\boldsymbol{v}$ for an arbitrary three-component vector $\boldsymbol{v}$, only two out of three Dirac cones will acquire a gap. In particular, the wave function $\Psi_\sigma(\tau, \boldsymbol{x}) \equiv m_\sigma \psi(\tau, \boldsymbol{x})$ will correspond to the massless Dirac fermions. The dynamical generation of such term hence corresponds to metallic quantum criticality in a Dirac system, in contrast to the situation in related models that feature metal-insulator transitions [33,38]. Equation (2) encodes a new class of Gross-Neveu (GN) transitions dubbed GN-SO(3) that have recently been studied using approximate analytical techniques [39].

The microscopic model (1) is amenable to large-scale negative-sign-free auxiliary-field quantum Monte Carlo (AFQMC) simulations [40–42], and Fig. 1 summarizes our key results at zero temperature and half band filling. In the weakly interacting limit, the model features a stable semimetallic phase, characterized by $N = 12$ irreducible Dirac cones located at the corners K and K' of the first Brillouin zone. At intermediate couplings, a semimetallic SO(3)-symmetry-broken phase with flavor order indeed emerges, in which two thirds of the Dirac cones are gapped out, while one third remains gapless. Remarkably, upon further increasing the interaction strength, we encounter another phase, which now is insulating and displays spontaneously broken U(1) symmetry, corresponding to emergent interlayer coherence. The first transition is continuous at the mean-field level, and the effects of quantum fluctuations can be understood in terms of the GN-SO(3) field theory studied in [39]. The second transition is strongly first order at the mean-field level, as is usual for direct transitions between states that break different symmetries. Our numerical results, however, indicate that quantum fluctuations render this order-to-order transition continuous (but we cannot exclude it to be weakly first order). It hence likely represents an example of a new type of deconfined quantum critical point [43] featuring gapless fermionic degrees of freedom [44].

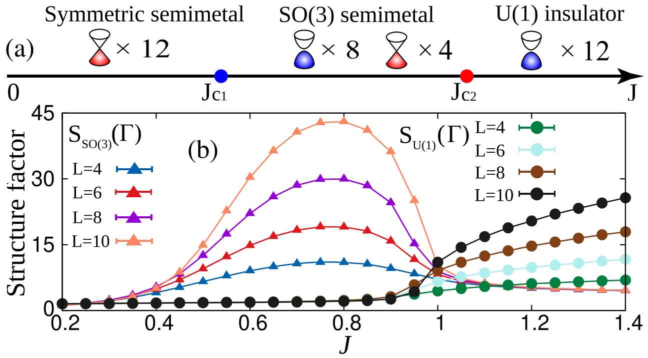

FIG. 1. (a) Ground-state phase diagram of the model (1) as function of interaction strength J, obtained from AFQMC simulations. The semimetal-to-semimetal transition at J_{c1} is continuous and can be understood in terms of a GN-SO(3) field theory. The semimetal-to-insulator transition at J_{c2}, while strongly first order at the mean-field level, appears continuous. (b) Variation of SO(3) and U(1) structure factors $S_{\mathrm{SO(3)}}(k=\Gamma)$ and $S_{\mathrm{U(1)}}(k=\Gamma)$ as function of J for different lattice sizes. Extensive structure factors reflect spontaneous symmetry breaking.

Mean-field analysis.—Our mean-field approximation relies on the identity

$$-J\sum_{i\alpha}(c_i^\dagger K^\alpha \tau^z c_i)^2 = -J\sum_{i\alpha\lambda}(c_{i\lambda}^\dagger K^\alpha c_{i\lambda})^2 + 2J\sum_{i\alpha\sigma\sigma'}|\epsilon_{\alpha\sigma\sigma'}|(\Delta_{i\sigma}^\dagger \Delta_{i\sigma'} + n_{i\sigma}^\dagger n_{i\sigma'}), \qquad (3)$$

with $\Delta_{i\sigma}^\dagger = c_{i\sigma 1}^\dagger c_{i\sigma 2}^\dagger$ and $n_{i\sigma}^\dagger = c_{i\sigma 1}^\dagger c_{i\sigma 2}$. The above allows us to define a SO(3) order parameter for staggered flavor order, $m_\alpha/2 = (-1)^{\boldsymbol{i}}\langle c_{i\lambda}^\dagger K^\alpha c_{i\lambda}\rangle$, and a U(1) order parameter for interlayer coherence, $V/2 = (-1)^{\boldsymbol{i}}\langle n_{i\sigma}^\dagger\rangle$. In the spirit of the continuum limit of Eq. (2), the order parameters map onto $\Psi_{\sigma\lambda}^\dagger \gamma_0 K_{\sigma\sigma'}^\alpha \Psi_{\sigma'\lambda}$ and $\Psi_{\sigma\lambda}^\dagger \gamma_0 \tau_{\lambda\lambda'}^x \Psi_{\sigma\lambda'}$, respectively, and open partial and full gaps in the fermion spectrum. Since in the quantum Monte Carlo (QMC) calculations we have not observed superconductivity, we omit the corresponding term in the mean-field approximation. For details of the calculations, see the Supplemental Material [45].

Figure 2(a) shows the mean-field order parameters as a function of J/t. The symmetric Dirac phase has a

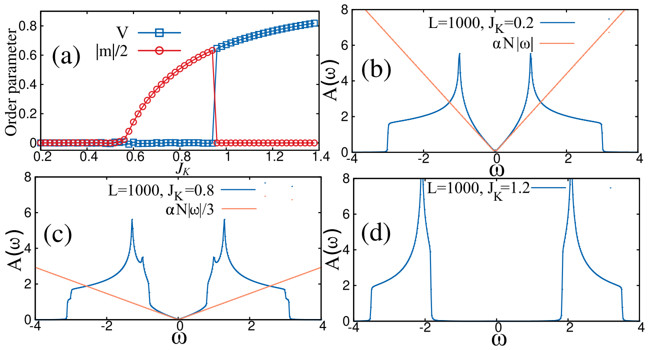

FIG. 2. Mean-field results for the model (1), obtained on a $L = 60$ lattice. (a) SO(3) and U(1) order parameters m_α and V as a function of J. (b)–(d) Single-particle density of states for representative fixed values of J in the three phases.

low-energy density of states $N(\omega) = \alpha N|\omega|$ that changes to $N(\omega) = \alpha(N/3)|\omega|$ in the SO(3)-broken phase, consistent with two out of three Dirac cones acquiring a mass gap, Figs. 2(b) and 2(c). At larger values of J/t, we observe a strong first-order transition to a U(1)-broken state whose fermion spectrum is gapped, Fig. 2(d).

QMC simulations.—We have used the ALF [47] implementation of AFQMC simulation and employed the finite-temperature grand canonical and projective approaches. We used a symmetric Suzuki-Trotter decomposition to control the systematic error in observables [48,49] and adopted an imaginary time step $\Delta\tau t = 0.05$ for the finite-temperature algorithm and $\Delta\tau t = 0.1$ for the projective formulation.

The absence of a negative-sign problem for positive values of J stems from a particular time-reversal symmetry that relies on the bilayer structure of the model. After a Hubbard-Stratonovich (HS) decomposition of the perfect-square interaction term, the resulting one-body Hamiltonian, for a given space-time configuration of HS fields, has a time-reversal symmetry, defined as $T^{-1} z c^{\dagger}_{i\sigma\lambda} T = \bar{z} i \tau^{y}_{\lambda\lambda'} c^{\dagger}_{i\sigma\lambda'}$. This stems from the fact that the SO(3) generators are purely imaginary. Hence, the eigenvalues of the fermion matrix occur in complex conjugate pairs such that positivity of the determinant follows [50]. To minimize size effects, we follow Ref. [51] and thread the lattice with a magnetic flux quantum of opposite sign in the two layers [45]. It is interesting to note that introducing a chemical potential will not break this time-reversal symmetry, and simulations at finite doping are amenable to negative-sign-free QMC.

QMC results.—We carry out QMC simulations of the model (1) on $L = 6$, 9, 12, 15, and 18 lattices with $6L^2$ orbitals per honeycomb layer, set $t = 1$, and scan as function of J. Our results are summarized schematically in Fig. 1(a). Each phase is characterized by spontaneous symmetry breaking and diverging structure factor at $\boldsymbol{Q} = \Gamma$, Fig. 1(b). To detect SO(3) symmetry breaking we consider $S_{\mathrm{SO(3)}}(\boldsymbol{k}, \tau) = \sum_{\boldsymbol{r}_{ij},\lambda} e^{-i\boldsymbol{k}\cdot\boldsymbol{r}_{ij}} \langle c^{\dagger}_{\boldsymbol{i},\lambda}(\tau) \boldsymbol{K} c_{\boldsymbol{i},\lambda}(\tau) \cdot c^{\dagger}_{\boldsymbol{j},\lambda}(0) \boldsymbol{K} c_{\boldsymbol{j},\lambda}(0) \rangle$ and, for the U(1) phase, $S_{\mathrm{U(1)}}(\boldsymbol{k}, \tau) = \frac{1}{2} \sum_{\boldsymbol{r}_{ij}\sigma} e^{-i\boldsymbol{k}\cdot\boldsymbol{r}_{ij}} \langle n^{\dagger}_{\boldsymbol{i},\sigma}(\tau) n_{\boldsymbol{j},\sigma} + n_{\boldsymbol{j},\sigma}(\tau) n^{\dagger}_{\boldsymbol{i},\sigma} \rangle$. Here, $\boldsymbol{r}_{ij}$ corresponds to the distance between the unit cells of $\boldsymbol{i}$ and $\boldsymbol{j}$.

Each phase has a distinct signature in the single-particle spectral function $A(\boldsymbol{k}, \omega)$. We extract this quantity from the ground-state imaginary-time-displaced fermion Green's functions $G(\boldsymbol{k}, \tau) = (1/\pi) \int d\omega e^{-\tau\omega} A(\boldsymbol{k}, \omega)$ by using the ALF [47] implementation of the stochastic analytic continuation method [52]. In Fig. 3(b), in the symmetric phase, the fermion spectrum reveals semimetallic behavior. In Fig. 3(c), in the SO(3)-broken phase, part of the low-energy spectral weight is removed, but a finite weight at the Dirac point is still apparent. To demonstrate this explicitly, we make use of the fact that, for a gapless mode, the quasiparticle residue reads $Z(\boldsymbol{k}) = 2\,\mathrm{Tr}\, G(\boldsymbol{k}, \beta/2)$ [53]. We use a $\beta = L$ scaling and extrapolate Z to the thermodynamic limit, see Fig. 3(a). In the semimetallic phase, the quasiparticle residue extrapolates to the free Dirac-metal value $Z(k = K) = 6$. In the SO(3)-symmetry-breaking phase, using a polynomial fit, we obtain the estimated quasiparticle residue $Z(k = K) = 1.9(1)$. The ratio of the quasiparticle weights is close to three, as expected from the gapping out of 2/3 of the Dirac cones. Finally in the U(1)-broken phase, the spectrum shows a full gap, Fig. 3(d).

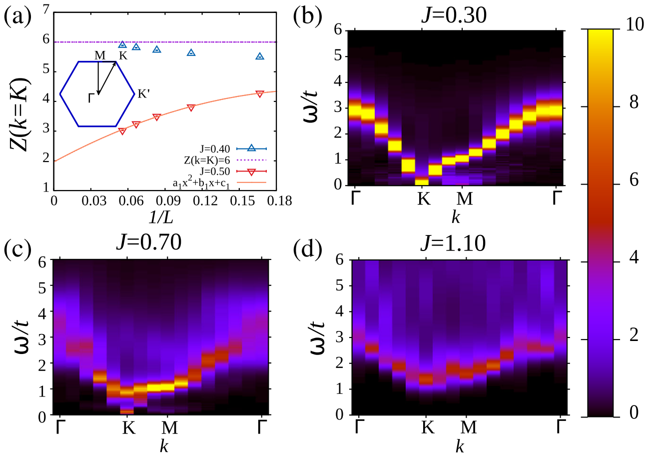

FIG. 3. (a) Quasiparticle weight $Z(k = K)$ as a function of inverse system size, $1/L$, in the symmetric ($J = 0.40$) and SO(3)-broken ($J = 0.50$) phases, respectively. The polynomial fitting of the second curve yields $Z = 1.9(1)$ for $L \to \infty$. (b)–(d) Fermion spectral function $A(\boldsymbol{k}, \omega)$ along the path in momentum space shown in the inset of (a), shown for (b) the symmetric phase at $J = 0.30$, (c) the SO(3)-broken phase at $J = 0.70$, and (d) the U(1)-broken phase at $J = 1.10$. Finite weight at the Dirac point is visible in (b) and (c), corresponding to semimetallic behavior, albeit with a reduced low-energy weight in the case of the SO(3)-broken semimetal (c). The low-energy weight at the M point especially visible in (b) is an artifact of the magnetic flux and does not survive the thermodynamic limit (see Supplemental Material [45]).

The two phase transition points are located by monitoring the renormalization-group invariant correlation ratio [54] $R_c = 1 - \{[S(\boldsymbol{k} = \boldsymbol{Q} + d\boldsymbol{k}, \tau = 0)]/[S(\boldsymbol{k} = \boldsymbol{Q}, \tau = 0)]\}$, where $S(\boldsymbol{k}, \tau = 0)$ is the structure factor of either the SO(3) or the U(1) order, $\boldsymbol{Q}$ is the ordering wave vector, and $d\boldsymbol{k}$ is the smallest momentum on the considered lattice.

To investigate the first phase transition, we will assume $z = 1$ and adopt a $\beta = L$ scaling within the finite-temperature AFQMC algorithm. As apparent in Fig. 4(a), this phase transition involves only SO(3) symmetry breaking since a clear crossing is observed in $R_c^{\mathrm{SO(3)}}$. On the other hand, $R_c^{\mathrm{U(1)}}$ vanishes for increasing system size, thus excluding long-range U(1) order in the considered parameter range. In the quantum critical region, we expect the correlation ratio $R_c^{\mathrm{SO(3)}}$ to obey the finite-size scaling (FSS) ansatz [55] $R_c^{\mathrm{SO(3)}}(J, L) = f_0^R(jL^{1/\nu}) + L^{-\omega} f_1^R(jL^{1/\nu})$,

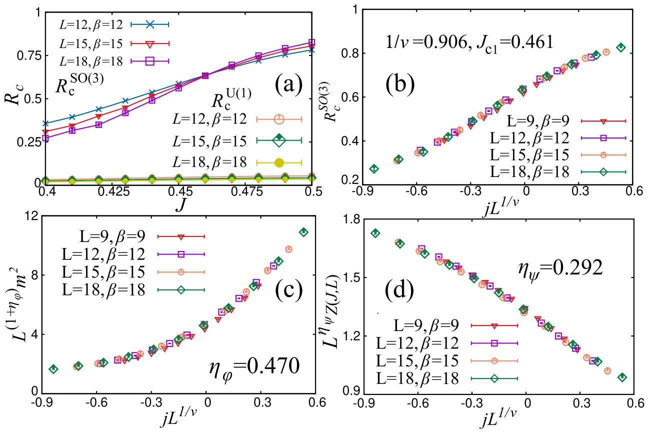

FIG. 4. QMC characterization of GN-SO(3) transition at J_{c1}. (a) Correlation ratios of the U(1) and SO(3) order parameters. (b)–(d) Scaling collapse near $J_{c1} = 0.461$ of (b) correlation ratio $R_c^{\mathrm{SO(3)}}$, (c) order parameter m^2, and (d) fermion quasiparticle weight Z, as a function of $jL^{1/\nu}$, with $j = J - J_{c1}$ and ν the correlation-length exponent.

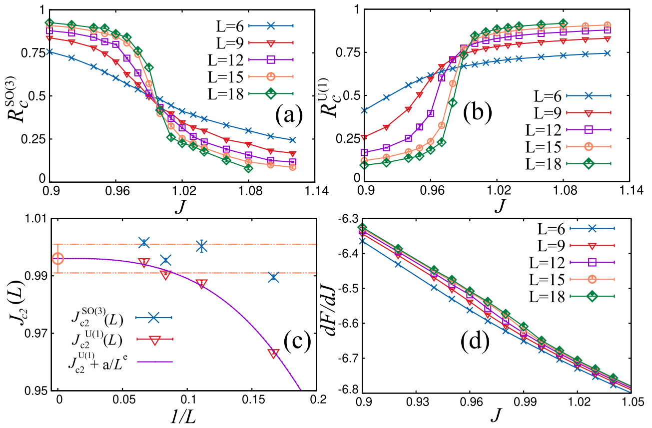

FIG. 5. QMC characterization of SO(3)-U(1) transition at J_{c2}. (a),(b) Correlation ratios as function of J across transition. (c) Finite-size critical couplings $J_{c2}^{\mathrm{SO(3)/U(1)}}(L)$ as a function of $1/L$. While $J_{c2}^{\mathrm{U(1)}}(L)$ increases with system size, $J_{c2}^{\mathrm{SO(3)}}(L)$ stabilizes within our accuracy as $L \geq 9$. By extrapolating $J_{c2}^{\mathrm{U(1)}}(L)$ using the power-law ansatz $J_{c2} + a/L^e$, we obtain the estimate $J_{c2} = 1.0013(18)$. (d) First derivative of free energy dF/dJ near J_{c2}, showing no discontinuity within our accuracy.

where $j = J - J_{c1}$. f_0^R and f_1^R are scaling functions and ω is the leading-correction-to-scaling exponent. To extract the values of the critical exponent ν and the critical point J_c, we fit the scaling function $f_0^R(jL^{1/\nu})$ to a polynomial [45]. In our simulations, the crossing point in the $R_c^{\mathrm{SO(3)}}$ data becomes size independent within our accuracy. Hence, for $L \geq 12$, corrections to scaling can be omitted. Our results are consistent with $1/\nu = 0.906(35)$ and $J_{c1} = 0.461(1)$. The data collapse of $R_c^{\mathrm{SO(3)}}(J,L)$ is depicted in Fig. 4(b). The bosonic η_ϕ and fermionic η_ψ anomalous dimensions are related to the FSS ansatz of the SO(3) order parameter $m^2 = S_{\mathrm{SO(3)}}(\mathbf{Q}, \tau = 0)/L^2$ and $Z(J,L) = G(J,L)/G(0,L)$, where $G(J,L) = \frac{1}{6}\sum_{\sigma,\lambda}\langle c^\dagger_{\mathbf{0}\sigma\lambda}(\beta/2)c_{\mathbf{0}\sigma\lambda}(0)\rangle$ at interaction strength J. At the critical point, and neglecting corrections to scaling, these two quantities scale as $m^2_{\mathrm{SO(3)}}(j,L) = L^{-(1+\eta_\phi)}f^m(jL^{1/\nu}) = L^{-(1+\eta_\phi)}\tilde{f}^m(R_c^{\mathrm{SO(3)}}(J,L))$ and $Z(J,L) = L^{-\eta_\psi}f^z(jL^{1/\nu}) = L^{-\eta_\psi}\tilde{f}^z(R_c^{\mathrm{SO(3)}}(J,L))$ [33]. Here we use the correlation ratio $R_c^{\mathrm{SO(3)}}(J,L)$ as a dimensionless quantity to replace the variable $jL^{1/\nu}$ so as to reduce the number of fit variables. Following the regression result of the scaling function, we obtain the estimates $\eta_\phi = 0.470(13)$ and $\eta_\psi = 0.292(10)$. Figures 4(c) and 4(d) show the data collapse using the estimated exponents. Consistent results are obtained when collapsing the data with respect to $jL^{1/\nu}$ with ν [45].

At the mean-field level, the transition between the SO(3)-broken and U(1)-broken states is strongly first order. However, the QMC results for $R_c^{\mathrm{SO(3)}}$ and $R_c^{\mathrm{U(1)}}$ do not suggest a strong first-order transition, Figs. 5(a) and 5(b). To assess if there is a coexistence regime, we carry out a crossing-point analysis to determine the coupling at which the SO(3) [U(1)] order is suppressed (appears). We determine the finite-size critical couplings $J_{c2}^{\mathrm{SO(3)/U(1)}}(L)$ by $R_c(J_{c2}(L), L) = R_c(J_{c2}(L), L+3)$. As the system size $L \to \infty$, the finite-size critical couplings $J_{c2}^{\mathrm{SO(3)/U(1)}}(L)$ scale as $J_{c2}^{\mathrm{SO(3)/U(1)}} + aL^{-e}$, where $e = 1/\nu + \omega$ and a is a nonuniversal constant. The results, plotted in Fig. 5(c), suggest that, within our accuracy, $J_{c2}^{\mathrm{SO(3)}} = J_{c2}^{\mathrm{U(1)}}$. In Fig. 5(d), we plot the first derivative of the free energy with respect to J. Within our accuracy, we do not observe a discontinuity expected for a first-order transition. Consistent estimates of the correlation-length exponent from the U(1) and SO(3) structure factors are reported in the Supplemental Material [45].

Discussion and summary.—We have introduced a model Hamiltonian, amenable to large-scale negative-sign-free QMC simulations, that supports metallic quantum criticality in Dirac systems. The SO(3) order generates mass in two out of three Dirac cones. Using a FSS analysis, we estimate the critical exponents of the SO(3)-ordering transition

$$1/\nu = 0.906(35), \quad \eta_\phi = 0.470(13), \quad \eta_\psi = 0.292(10) \qquad (4)$$

for the correlation-length exponent and the boson and fermion anomalous dimensions. We expect our model to fall into the GN-SO(3) universality class, with $N = 12$ two-component Dirac fermions. Calculations in [39], based on ϵ expansion, large-N, and functional renormalization-group approaches, yield exponents that differ from our estimates: $1/\nu = 0.93(4)$, $\eta_\phi = 0.83(4)$, and $\eta_\psi = 0.041(12)$. While we cannot exclude that the discrepancy stems from finite-size effects in the QMC or convergence issues in the analytical approaches, they are large enough to speculate if topological defects in the field configurations—not included in [39]—play a role, see below. Note that within the QMC approach one can, in principle, systematically carry out calculations at $N = 12n$ and thereby test the validity of the large-N approach.

At larger couplings, the model shows an order-to-order transition between the SO(3) semimetal and a U(1) insulator. While at the mean-field level this transition is strongly first order, the QMC data on lattice sizes with up to 18×18 unit cells can be interpreted in terms of a continuous and direct transition, thereby providing an instance of a new type of deconfined quantum critical point [43] featuring gapless fermionic degrees of freedom [44]. Clearly, we cannot exclude the possibility of a weakly first-order transition, in which, as suggested in the realm of deconfined criticality, the correlation length grows beyond the accessible system size due to the proximity of a critical fixed point in the complex-coupling plane [56–62].

The discrepancy between the QMC critical exponents and those of Ref. [39], as well as the seemingly continuous transition between the SO(3)-broken semimetal and U(1)-broken insulator, leads us to ask the question if the topology of the SO(3) order parameter can play a role. For a given SO(3) mass term, $[\boldsymbol{m}(\boldsymbol{x}) \cdot \boldsymbol{K}]\gamma_0$, the wave function of the gapless Dirac cone reads $\Psi_{\sigma\lambda}(\boldsymbol{x}) = m_\sigma(\boldsymbol{x})\psi_\lambda(\boldsymbol{x})$. Consider an interface where on both sides the vectors $\boldsymbol{m}$ are orthogonal to each other. Because of the orthogonality of the vectors $\boldsymbol{m}$, the wave function vanishes at the interface and a particle will not be able to cross it. The topological excitation of the SO(3) order parameter in two spatial dimensions is a skyrmion. In its core the SO(3) order parameter is given by $\boldsymbol{m}_c$ and at infinity by $-\boldsymbol{m}_c$. The core is surrounded by a vortex in a plane perpendicular to $\boldsymbol{m}_c$ that acts as an infinite potential barrier. As a consequence, we can foresee that a skyrmion of the SO(3) order parameter will trap charge in its core. Mean calculations supporting this point of view are presented in the Supplemental Material [45]. Understanding if this "topological localization" is essential for the description of the observed phase transitions remains an open issue.

The phase diagram of our model contains two ordered phases with low-lying Goldstone modes. As mentioned above, it is possible to dope our system without encountering a negative-sign problem. Hence, numerical simulations aimed at understanding the nature of the doping-induced transitions to correlated metals (or superconductors [63]) should be feasible; these will be the subject of future work.

The authors gratefully acknowledge the Gauss Centre for Supercomputing e.V. (www.gauss-centre.eu) for funding this project by providing computing time on the GCS Supercomputer SUPERMUC-NG at Leibniz Supercomputing Centre (www.lrz.de). This research has been supported by the Deutsche Forschungsgemeinschaft through the Würzburg-Dresden Cluster of Excellence on Complexity and Topology in Quantum Matter—ct.qmat (EXC 2147, Project No. 390858490), SFB 1170 on Topological and Correlated Electronics at Surfaces and Interfaces (Project No. 258499086), SFB 1143 on Correlated Magnetism (Project No. 247310070), and the Emmy Noether Program (JA2306/4-1, Project No. 411750675).

[1] J. A. Hertz, Phys. Rev. B **14**, 1165 (1976).
[2] A. J. Millis, Phys. Rev. B **48**, 7183 (1993).
[3] T. Moriya, *Spin Fluctuations in Itinerant Electron Magnetism* (Springer, Berlin, 2012).
[4] W. Metzner, D. Rohe, and S. Andergassen, Phys. Rev. Lett. **91**, 066402 (2003).
[5] T. Senthil, Phys. Rev. B **78**, 035103 (2008).
[6] H. v. Löhneysen, A. Rosch, M. Vojta, and P. Wölfle, Rev. Mod. Phys. **79**, 1015 (2007).
[7] P. Gegenwart, Q. Si, and F. Steglich, Nat. Phys. **4**, 186 (2008).
[8] B. Keimer, S. A. Kivelson, M. R. Norman, S. Uchida, and J. Zaanen, Nature (London) **518**, 179 (2015).
[9] T. Shibauchi, A. Carrington, and Y. Matsuda, Annu. Rev. Condens. Matter Phys. **5**, 113 (2014).
[10] A. Abanov, A. V. Chubukov, and J. Schmalian, Adv. Phys. **52**, 119 (2003).
[11] A. Abanov and A. Chubukov, Phys. Rev. Lett. **93**, 255702 (2004).
[12] M. A. Metlitski and S. Sachdev, Phys. Rev. B **82**, 075127 (2010).
[13] M. A. Metlitski and S. Sachdev, Phys. Rev. B **82**, 075128 (2010).
[14] S. Sur and S.-S. Lee, Phys. Rev. B **94**, 195135 (2016).
[15] A. Schlief, P. Lunts, and S.-S. Lee, Phys. Rev. X **7**, 021010 (2017).
[16] S.-S. Lee, Annu. Rev. Condens. Matter Phys. **9**, 227 (2018).
[17] A. Schlief, P. Lunts, and S.-S. Lee, Phys. Rev. B **98**, 075140 (2018).
[18] A. Chubukov, J. Club Condens. Matter Phys. (2018).
[19] X. Y. Xu, A. Klein, K. Sun, A. V. Chubukov, and Z. Y. Meng, npj Quantum Mater. **5**, 1 (2020).
[20] J. Zinn-Justin, Nucl. Phys. **B367**, 105 (1991).
[21] F. Gehring, H. Gies, and L. Janssen, Phys. Rev. D **92**, 085046 (2015).
[22] N. Zerf, L. N. Mihaila, P. Marquard, I. F. Herbut, and M. M. Scherer, Phys. Rev. D **96**, 096010 (2017).
[23] J. A. Gracey, Phys. Rev. D **97**, 105009 (2018).
[24] L. Iliesiu, F. Kos, D. Poland, S. S. Pufu, and D. Simmons-Duffin, J. High Energy Phys. 01 (2018) 36.
[25] E. Huffman and S. Chandrasekharan, Phys. Rev. D **101**, 074501 (2020).
[26] I. F. Herbut, Phys. Rev. Lett. **97**, 146401 (2006).
[27] I. F. Herbut and V. Juričič, and O. Vafek, Phys. Rev. B **80**, 075432 (2009).
[28] L. Janssen and I. F. Herbut, Phys. Rev. B **89**, 205403 (2014).
[29] F. F. Assaad and I. F. Herbut, Phys. Rev. X **3**, 031010 (2013).

[30] F. Parisen Toldin, M. Hohenadler, F. F. Assaad, and I. F. Herbut, Phys. Rev. B **91**, 165108 (2015).

[31] Y. Otsuka, K. Seki, S. Sorella, and S. Yunoki, Phys. Rev. B **98**, 035126 (2018).

[32] T. C. Lang and A. M. Läuchli, Phys. Rev. Lett. **123**, 137602 (2019).

[33] Y. Liu, Z. Wang, T. Sato, M. Hohenadler, C. Wang, W. Guo, and F. F. Assaad, Nat. Commun. **10**, 1 (2019).

[34] Y. Liu, W. Wang, K. Sun, and Z. Y. Meng, Phys. Rev. B **101**, 064308 (2020).

[35] X. Y. Xu and T. Grover, Phys. Rev. Lett. **126**, 217002 (2021).

[36] Y. Liu, Z. Wang, T. Sato, W. Guo, and F. F. Assaad, Phys. Rev. B **104**, 035107 (2021).

[37] U. F. P. Seifert, X.-Y. Dong, S. Chulliparambil, M. Vojta, H.-H. Tu, and L. Janssen, Phys. Rev. Lett. **125**, 257202 (2020).

[38] Z. Wang, Y. Liu, T. Sato, M. Hohenadler, C. Wang, W. Guo, and F. F. Assaad, Phys. Rev. Lett. **126**, 205701 (2021).

[39] S. Ray, B. Ihrig, D. Kruti, J. A. Gracey, M. M. Scherer, and L. Janssen, Phys. Rev. B **103**, 155160 (2021).

[40] R. Blankenbecler, D. J. Scalapino, and R. L. Sugar, Phys. Rev. D **24**, 2278 (1981).

[41] J. E. Hirsch, Phys. Rev. B **31**, 4403 (1985).

[42] S. R. White, D. J. Scalapino, R. L. Sugar, E. Y. Loh, J. E. Gubernatis, and R. T. Scalettar, Phys. Rev. B **40**, 506 (1989).

[43] T. Senthil, L. Balents, S. Sachdev, A. Vishwanath, and M. P. A. Fisher, Phys. Rev. B **70**, 144407 (2004).

[44] L. Zou and D. Chowdhury, Phys. Rev. Research **2**, 023344 (2020).

[45] See Supplemental Material at http://link.aps.org/supplemental/10.1103/PhysRevLett.128.087201 for technical details of the mean-field calculation, the effects of magnetic flux on the spectral function, and finite-size scaling analyses, as well as a discussion of electron localization effects of topological defects of the SO(3) order parameter, which includes Ref. [63].

[46] H. Shao, W. Guo, and A. W. Sandvik, Science **352**, 213 (2016).

[47] F. F. Assaad, M. Bercx, F. Goth, A. Götz, J. S. Hofmann, E. Huffman, Z. Liu, F. Parisen Toldin, J. S. E. Portela, and J. Schwab (ALF Collaboration), arXiv:2012.11914.

[48] M. Suzuki, Commun. Math. Phys. **51**, 183 (1976).

[49] H. F. Trotter, Proc. Am. Math. Soc. **10**, 545 (1959).

[50] C. Wu and S.-C. Zhang, Phys. Rev. B **71**, 155115 (2005).

[51] F. F. Assaad, Phys. Rev. B **65**, 115104 (2002).

[52] K. Beach, arXiv:cond-mat/0403055.

[53] M. Brunner, F. F. Assaad, and A. Muramatsu, Phys. Rev. B **62**, 15480 (2000).

[54] R. K. Kaul, Phys. Rev. Lett. **115**, 157202 (2015).

[55] M. Campostrini, A. Pelissetto, and E. Vicari, Phys. Rev. B **89**, 094516 (2014).

[56] A. Nahum, J. T. Chalker, P. Serna, M. Ortuño, and A. M. Somoza, Phys. Rev. X **5**, 041048 (2015).

[57] C. Wang, A. Nahum, M. A. Metlitski, C. Xu, and T. Senthil, Phys. Rev. X **7**, 031051 (2017).

[58] P. Serna and A. Nahum, Phys. Rev. B **99**, 195110 (2019).

[59] A. Nahum, Phys. Rev. B **102**, 201116(R) (2020).

[60] R. Ma and C. Wang, Phys. Rev. B **102**, 020407(R) (2020).

[61] V. Gorbenko, S. Rychkov, and B. Zan, J. High Energy Phys. 10 (2018) 108.

[62] V. Gorbenko, S. Rychkov, and B. Zan, SciPost Phys. **5**, 50 (2018).

[63] V. Kozii, Z. Bi, and J. Ruhman, Phys. Rev. X **9**, 031046 (2019).